J. Fluid Mech. (2003), *vol.* 479, *pp.* 199–219.
DOI: 10.1017/S0022112002003506 Printed in the United Kingdom

An improved exact Riemann solver for multi-dimensional relativistic flows

By LUCIANO REZZOLLA[1,2], OLINDO ZANOTTI[1] AND JOSE A. PONS[3]

[1]SISSA, International School for Advanced Studies, Trieste, Via Beirut 2–4, 34014 Trieste, Italy

[2]INFN, Physics Department, University of Trieste, Via Valerio 2, 34127 Trieste, Italy

[3]Physics Department, University of Rome 'La Sapienza', Piazzale Aldo Moro 2, I-00185 Rome, Italy

(Received 15 May 2002 and in revised form 23 October 2002)

We extend our approach for the exact solution of the Riemann problem in relativistic hydrodynamics to the case in which the fluid velocity has components tangential to the initial discontinuity. As in one-dimensional flows, we show here that the wave pattern produced in a Riemann problem with multi-dimensional relativistic flows can be predicted entirely by examining the initial conditions. Our method is logically very simple and allows for a numerical implementation of an exact Riemann solver which is both straightforward and computationally efficient. The simplicity of the approach is also important for revealing special relativistic effects responsible for a smooth transition from one wave pattern to another when the tangential velocities in the initial states are suitably varied. Although this paper is focused on a flat space–time, the local Lorentz invariance allows its use also in fully general relativistic calculations.

1. Introduction

Since the solution of the Riemann problem was introduced in numerical hydrodynamics (Godunov 1959), high-resolution shock capturing methods have become a common tool for handling nonlinear hydrodynamical waves in a variety of physical situations and the subject of detailed mathematical analyses both in Newtonian (Leveque 1992, 2002; Toro 1997) and relativistic regimes (Smoller & Temple 1993). Nonlinear waves of this type are very common in astrophysical scenarios (such as gamma-ray bursts, accretion onto compact objects, relativistic jets, supernova explosions) in which the motion of the fluid is characterized by relativistic speeds and by the appearance of strong discontinuities (see Ibañez & Martí 1999; Martí & Müller 1999; for a review). Rezzolla & Zanotti (2001 hereinafter referred to as paper I) proposed a new procedure for the exact solution of the Riemann problem which uses the relativistically invariant relative velocity between the unperturbed 'left' and 'right' states of the fluid. They extracted important information contained in the initial data that more traditional approaches were not able to put into evidence. Most notably, it was shown that, given a Riemann problem with assigned initial conditions, it is possible to determine in advance both the wave pattern that will be produced after the removal of the initial planar discontinuity and the bracketing interval of the unknown pressure in the region that forms behind the wavefronts. Besides clarifying some aspects of the Riemann problem, the approach proposed by Rezzolla & Zanotti, and that was foreseen by Landau & Lifshitz (1987) in Newtonian hydrodynamics,

was shown to be computationally more efficient as compared to the more traditional approaches.

The analytic solution of the one-dimensional Riemann problem (Martí & Müller 1994) has been extended recently to the case in which non-zero velocities tangential to the initial planar discontinuity are present (Pons, Martí & Müller 2000). An important result obtained by Pons *et al.* (2000) was to show that the introduction of tangential velocities and the appearance of global Lorentz factors linking quantities on either side of the discontinuity can affect the solution of the Riemann problem considerably. In the present paper, we show that the approach by Rezzolla & Zanotti can be successfully extended to this more general case and with the same advantages that were found in the case of zero tangential velocities. Within this new procedure, the introduction of tangential velocities is imprinted in the expression for the jump of the velocity normal to the discontinuity surface, and this has allowed us to reveal interesting special relativistic effects. In relativistic hydrodynamics, in fact, the wave pattern produced by the decay of the initial discontinuity can be changed by simply varying the tangential velocities in the initial states, while keeping the rest of the thermodynamic quantities of the Riemann problem unmodified. This effect has no analogue in Newtonian hydrodynamics (Rezzolla & Zanotti 2002).

The plan of the paper is as follows. After a review of the method in § 2, we report in § 3 the hydrodynamical equations relevant for the present discussion of non-zero tangential velocities. In § 4, we show how to use the invariant relative velocity to extract from the initial data the information on the wave pattern produced, while § 5 is devoted to the presentation of the special relativistic effects. The conclusions of the paper are in § 6, and three Appendices complete the discussion providing the mathematical details of the results obtained in the main text.

We use in this paper a system of units in which $c = 1$, a space-like signature $(-, +, +, +)$ and a Cartesian coordinate system (t, x, y, z). Greek indices are taken to run from 0 to 3, Latin indices from 1 to 3 and we adopt the standard convention for the summation over repeated indices.

2. A brief review of the method

In a flat space–time consider a perfect fluid described by the stress-energy tensor

$$T^{\mu\nu} \equiv (e + p)u^\mu u^\nu + p\eta^{\mu\nu} = \rho h u^\mu u^\nu + p\eta^{\mu\nu}, \tag{2.1}$$

where $\eta^{\mu\nu} = \mathrm{diag}(-1, 1, 1, 1)$ and e, p, ρ and h are the proper energy density the isotropic pressure, the proper rest-mass density and the specific enthalpy, respectively. The evolution of the fluid is described by the relativistic Euler equations ensuring the conservation of energy and momentum

$$T^{\mu\nu}_{\ \ ,\nu} = 0, \tag{2.2}$$

as well as the conservation of baryon number

$$(\rho u^\mu)_{,\mu} = 0. \tag{2.3}$$

The set of equations (2.2) and (2.3) is closed after an equation of state (EOS) is specified which relates the pressure to the rest-mass density or other thermodynamical quantities. The numerical solution of the set of relativistic hydrodynamic equations (2.2) and (2.3) is particularly convenient when these are written in the conservative form

$$\boldsymbol{U}_{,t} + \boldsymbol{F}^{(i)}_{,i} = 0 \tag{2.4}$$

where $\boldsymbol{U}$ is the vector of *conserved variables*, with components

$$\boldsymbol{U} \equiv (D, S^j, \tau)^T \qquad (j = 1, 2, 3), \tag{2.5}$$

and $\boldsymbol{F}^{(i)} = \boldsymbol{F}^{(i)}(\boldsymbol{U})$ are the vectors of fluxes, with components

$$\boldsymbol{F}^{(i)} \equiv (Dv^i, S^j v^i + p\delta^{ji}, S^i - Dv^i)^T \qquad (i, j = 1, 2, 3). \tag{2.6}$$

The conserved variables D, S^i and τ are defined in terms of the *primitive variables* ρ, v^i and ϵ, according to the following set of non-invertible relations

$$D \equiv \rho W, \tag{2.7}$$

$$S^i \equiv \rho h W^2 v^i, \tag{2.8}$$

$$\tau \equiv \rho h W^2 - p - D. \tag{2.9}$$

Assume now the fluid to consist of an initial 'left' state (indicated with an index 1) and an initial 'right' state (indicated with an index 2), each having prescribed and different values of uniform pressure, rest-mass density and velocity. The two discontinuous states are initially separated by a planar hypersurface Σ_0 placed at a constant value of the x coordinate so that the unit space-like four-vector n_0^μ normal to this surface at $t = 0$ has components $n_0^\mu \equiv (0, 1, 0, 0)$. Notice that, in contrast with Newtonian hydrodynamics, in special relativity, this surface Σ_0 is of constant time only for the set of inertial frames connected by a boost in the direction normal to the initial discontinuity or by spatial rotations. In a different set of inertial frames, in fact, a hypersurface of constant time consisting of a single initial discontinuity separating two constant states will not exist. Rather, the 'initial states' will be more complex and reflect the rich structure of the solution of the Riemann problem.

Because we are considering a multi-dimensional flow, the fluid four-velocity on either side of the initial discontinuity is allowed to have components in spatial directions orthogonal to n_0^μ, i.e.

$$u^\mu \equiv W(1, v^x, v^y, v^z), \tag{2.10}$$

where $W^2 = (1 - v^2)^{-1}$ is the square of the Lorentz factor and $v^2 \equiv v^i v_i = (v^x)^2 + (v^y)^2 + (v^z)^2$ is the norm of the three-velocity. As a result, the initial left and right fluid states are completely described in terms of the 'state vectors'

$$\boldsymbol{Q}_{1,2}(x) = \left(p, \rho, v^x, v^t\right)^T_{1,2}, \tag{2.11}$$

where we have indicated with $v^t \equiv [(v^y)^2 + (v^z)^2]^{1/2}$ the *tangential* component of the three-velocity, satisfying the obvious relativistic constraint that $(v^t)^2 + (v^x)^2 \leqslant 1$. Hereinafter, we will refer to v^x as the *normal* velocity.

Within this framework, the fluid states $\boldsymbol{Q}_1(x)$ and $\boldsymbol{Q}_2(x)$ represent the initial conditions of a Riemann problem with multi-dimensional relativistic flows, that is, of a Riemann problem whose initial states depend on one spatial coordinate only, but where the velocity is relativistic and has more than one non-zero component. The solution to this problem consists of determining the flow that develops when the system is allowed to relax. In general, the temporal evolution can be indicated as (Martí & Müller 1994)

$$L\mathscr{W}_{\leftarrow}L_*\mathscr{C}R_*\mathscr{W}_{\rightarrow}R, \tag{2.12}$$

where $\mathscr{W}$ denotes a nonlinear wave (either a shock, $\mathscr{S}$, or a rarefaction wave, $\mathscr{R}$), propagating towards the left ($\leftarrow$) or the right ($\rightarrow$) with respect to the initial discontinuity. Moreover, L_* and R_* are the new hydrodynamic states that form behind

the two nonlinear waves propagating in opposite directions. A contact discontinuity, $\mathscr{C}$, separates the region L_* and R_*, and it is characterized by the fact that both the pressure and the normal velocity are continuous across it, whereas both the rest-mass density and the tangential velocities can be discontinuous.

The new approach, first introduced in paper I, focuses on $(v^x_{12})_0$, the relativistic invariant expression for the initial relative velocity between the two unperturbed initial states. By construction, this quantity measures the relativistic jump of the fluid velocity normal to the discontinuity surface. The solution of the relativistic Riemann problem is then found after the pressure in the region between the two nonlinear waves, p_*, is calculated as the root of the nonlinear equation

$$v^x_{12}(p_*) - \left(v^x_{12}\right)_0 = 0, \tag{2.13}$$

where $v^x_{12}(p_*)$ has a functional form that is *different* for each of the *three* possible wave patterns that might result from the decay of the initial discontinuity. The key feature of the new approach is that the wave pattern produced by the decay of the initial discontinuity can be entirely predicted in terms of the initial data $\boldsymbol{Q}_{1,2}$. This represents an important advantage since it allows us to deduce in advance which set of equations to use for the solution of the exact Riemann problem and the interval bracketing the root of (2.13) (see paper I for details on the numerical implementation of the new approach). This, in turn, translates into a simpler logical formulation of the Riemann problem and into more efficient numerical algorithms with a reduction of the computational costs. Furthermore, and as we shall discuss in § 5, this new strategy has been essential in revealing new special relativistic effects.

The extension of the approach presented in paper I to the case when tangential velocities are present is straightforward since in this case also the expression for the normal relative velocity v^x_{12} is invariant under a Lorentz boost in the x-direction (i.e. a special Lorentz transformation). As a result, (2.13) as well as the logical scheme presented in paper I apply unmodified. The only changes introduced by the presence of tangential velocities are restricted to the expressions for the limiting values of the relative velocity $(\tilde{v}^x_{12})_{2S}$, $(\tilde{v}^x_{12})_{SR}$ and $(\tilde{v}^x_{12})_{2R}$. The details of these changes will be presented in the following sections which have been written for a generic EOS and use an ideal fluid EOS as a test case.

3. Hydrodynamical relations across the waves

As discussed in § 2, the expression for the relative normal velocity between the two initial states of the Riemann problem represents the building block in our approach and, to simplify our notation, hereinafter we will refer to the different flow regions using the following mapping

$$L\mathscr{W}_{\leftarrow}L_*\mathscr{C}R_*\mathscr{W}_{\rightarrow}R \Longleftrightarrow 1\ \mathscr{W}_{\leftarrow}\ 3\ \mathscr{C}\ 3'\ \mathscr{W}_{\rightarrow}\ 2, \tag{3.1}$$

so that, for instance, $p_* = p_3 = p_{3'}$.

While the values of v^x_{12} are relativistic invariants under a Lorentz boost in the x-direction, there exists a reference frame which is better suited to evaluate this quantity. In the reference frame of the contact discontinuity, in fact, the normal velocities behind the nonlinear waves are, by definition, zero (i.e. $v^x_{3,\mathscr{C}} = 0 = v^x_{3',\mathscr{C}}$) and the relative velocities across the nonlinear waves measured in this reference frame will be

$$\left(v^x_{13}\right)_{,\mathscr{C}} \equiv \frac{v^x_{1,\mathscr{C}} - v^x_{3,\mathscr{C}}}{1 - \left(v^x_{1,\mathscr{C}}\right)\left(v^x_{3,\mathscr{C}}\right)} = v^x_{1,\mathscr{C}}, \tag{3.2}$$

$$\left(v^x_{23'}\right)_{,\mathscr{C}} \equiv \frac{v^x_{2,\mathscr{C}} - v^x_{3',\mathscr{C}}}{1 - \left(v^x_{2,\mathscr{C}}\right)\left(v^x_{3',\mathscr{C}}\right)} = v^x_{2,\mathscr{C}}. \tag{3.3}$$

Because of their invariance to Lorentz boosts in the x-direction, the normal velocity jumps across the nonlinear waves measured in the Eulerian frame can be expressed as

$$\left(v^x_{13}\right) = \frac{v^x_1 - v^x_3}{1 - v^x_1 v^x_3} = \left(v^x_{13}\right)_{,\mathscr{C}} = v^x_{1,\mathscr{C}}, \tag{3.4}$$

$$\left(v^x_{23'}\right) = \frac{v^x_2 - v^x_{3'}}{1 - v^x_2 v^x_{3'}} = \left(v^x_{23'}\right)_{,\mathscr{C}} = v^x_{2,\mathscr{C}}. \tag{3.5}$$

As a result, the relative normal velocity between the two initial states can be written as

$$v^x_{12} = \left(v^x_{12}\right)_{,\mathscr{C}} = \frac{v^x_{1,\mathscr{C}} - v^x_{2,\mathscr{C}}}{1 - \left(v^x_{1,\mathscr{C}}\right)\left(v^x_{2,\mathscr{C}}\right)}. \tag{3.6}$$

In what follows, we will briefly discuss how to calculate the normal velocity jump across a shock wave and a rarefaction wave, respectively. The expressions derived in this way will then be used to calculate $v^x_{1,\mathscr{C}}$ and $v^x_{2,\mathscr{C}}$ necessary to build $v^x_{12} = v^x_{12}(p_*)$ (cf. (3.6)).

3.1. *Jumps across a shock wave*

Calculating jump conditions in the rest frame of the shock front is not particularly advantageous when tangential velocities are present. In this case, in fact, the velocity jump across the shock cannot be expressed as an algebraic relation among the thermodynamical quantities across the shock (cf. (3.1) of paper I). Rather, the ratio of the velocities ahead of and behind the shock front must be found as a root of a nonlinear equation (Koenigl 1980). For this reason, it is more convenient to use the Rankine–Hugoniot conditions in the Eulerian reference frame. In particular, adopting the standard notation in which the difference of a quantity evaluated behind (subscript b) and ahead (subscript a) of the wave is denoted as $[[F]] \equiv F_a - F_b$ (Anile 1989), these conditions can be expressed as (see also Pons *et al.* 2000)

$$[[v^x]] = -\frac{J}{W_s}[[1/D]], \tag{3.7}$$

$$[[p]] = \frac{J}{W_s}[[S^x/D]], \tag{3.8}$$

$$[[S^y/D]] = 0 = [[S^z/D]], \tag{3.9}$$

$$[[v^x p]] = \frac{J}{W_s}[[\tau/D]]. \tag{3.10}$$

In (3.7), (3.8) and (3.10), J represents the invariant (under Lorentz boosts in the x-direction) mass flux across the shock

$$J \equiv W_s D_a\left(V_s - v^x_a\right) = W_s D_b\left(V_s - v^x_b\right), \tag{3.11}$$

and $W_s \equiv (1 - V_s^2)^{-1/2}$ is the Lorentz factor of the shock velocity V_s, with the latter being

$$V_s^{\pm} = \frac{\rho_a^2 W_a^2 v^x_a \pm |J|\sqrt{J^2 + \rho_a^2 W_a^2\left[1 - \left(v^x_a\right)^2\right]}}{\rho_a^2 W_a^2 + J^2}, \tag{3.12}$$

and with the $\pm$ signs referring to a shock wave propagating to the right or to the left, respectively.

We can now exploit (3.7)–(3.10) to express the normal velocity of the fluid on the back of the shock front in terms of the pressure as

$$v_b^x = \frac{h_a W_a v_a^x + W_s(p_b - p_a)/J}{h_a W_a + (p_b - p_a)\left[W_s v_a^x/J + 1/(\rho_a W_a)\right]}. \tag{3.13}$$

Besides giving the jump in the normal velocity across a shock wave, (3.13) states that the two regions of the flow across the shock wave are coupled through a Lorentz factor which, we recall, is also built in terms of the tangential velocities. This is a purely relativistic feature and an important difference from Newtonian hydrodynamics, in which the solution of the Riemann problem does not depend on the tangential component of the flow. Some of the consequences introduced by this coupling will be further discussed in § 5, but one of them can be deduced immediately from (3.9), indicating that the ratio v^y/v^z remains unchanged through shocks so that the tangential velocity three-vector does not rotate, but can change its norm. This property, which applies also across rarefaction waves, represents a major difference from the behaviour of the tangential three-velocity vector across Newtonian nonlinear waves, which does not rotate, or change its norm: $[[v^y]] = 0 = [[v^z]]$.

The square of the mass flux across the wave can be expressed as

$$J^2 = -\frac{[[p]]}{[[h/\rho]]}, \tag{3.14}$$

where the ratio h/ρ in the shocked region can be calculated through the Taub adiabat (Taub 1948)

$$[[h^2]] = \left(\frac{h_a}{\rho_a} + \frac{h_b}{\rho_b}\right)[[p]]. \tag{3.15}$$

In a general case, the mass flux can be obtained as a function of just one thermodynamical variable (p_*) after using the EOS and the physical ($h \geqslant 1$) solution of the nonlinear equation (3.15). In the case of an ideal fluid EOS,

$$p = (\gamma - 1)\rho\epsilon = k(s)\rho^\gamma, \tag{3.16}$$

where γ is the adiabatic index, and $k(s)$ is the polytropic constant (dependent only on the specific entropy s), this can be done explicitly because (3.14) and (3.15) take, respectively, the simple form

$$J^2 = -\frac{\gamma}{\gamma - 1}\frac{[[p]]}{[[h(h-1)/p]]}, \tag{3.17}$$

and

$$\left[1 + \frac{(\gamma - 1)(p_a - p_b)}{\gamma p_b}\right] h_b^2 - \frac{(\gamma - 1)(p_a - p_b)}{\gamma p_b} h_b + \frac{h_a(p_a - p_b)}{\rho_a} - h_a^2 = 0. \tag{3.18}$$

3.2. *Jumps across a rarefaction wave*

When considering a rarefaction wave, it is convenient to introduce the self-similar variable $\xi \equiv x/t$ in terms of which similarity solutions to the hydrodynamical equations can be found. An explicit expression for ξ can be obtained by requiring that non-trivial similarity solutions for the rarefaction wave exist. This then yields

(see Pons *et al.* 2000 for details)

$$\xi = \frac{v^x\left(1-c_s^2\right) \pm c_s\sqrt{\left(1-v^2\right)\left[1-v^2c_s^2-(v^x)^2\left(1-c_s^2\right)\right]}}{1-v^2c_s^2}, \tag{3.19}$$

where here, too, the $\pm$ signs correspond to rarefaction waves propagating to the right or to the left, respectively. In the case of a perfect fluid, the isentropic character of the flow allows us to calculate the velocity on the back of the wave as a solution of an ordinary differential equation

$$\frac{\mathrm{d}v^x}{\mathrm{d}p} = \frac{1}{\rho h W^2}\frac{(1-\xi v^x)}{(\xi - v^x)}, \tag{3.20}$$

In principle, to calculate the normal fluid velocity at the tail of the rarefaction wave, we should solve the ordinary differential equation (3.20), which might be very expensive numerically. To overcome this, it is convenient to make use of constraints such as those in (3.9) (which remain valid also across a rarefaction wave) and express (3.20) in a different way. Defining $\mathscr{A} \equiv h_a W_a v_a^t = h_b W_b v_b^t$ (Pons *et al.* 2000), the tangential velocity along a rarefaction wave can be expressed as

$$(v^t)^2 = \mathscr{A}^2\left[\frac{1-(v^x)^2}{h^2+\mathscr{A}^2}\right]. \tag{3.21}$$

This allows us to eliminate the dependence on v^t from (3.19). From the definition of the Lorentz factor and (3.21) it is straightforward to obtain

$$W^2 = \frac{h^2+\mathscr{A}^2}{h^2[1-(v^x)^2]}, \tag{3.22}$$

and after some algebra, we can arrive at

$$\frac{(1-\xi v^x)}{(\xi - v^x)} = \pm\frac{\sqrt{h^2+\mathscr{A}^2\left(1-c_s^2\right)}}{hc_s}. \tag{3.23}$$

Using this results, (3.20) can be written as follows:

$$\frac{\mathrm{d}v^x}{1-(v^x)^2} = \pm\frac{\sqrt{h^2+\mathscr{A}^2\left(1-c_s^2\right)}}{(h^2+\mathscr{A}^2)}\frac{\mathrm{d}p}{\rho\ c_s}, \tag{3.24}$$

Note that, in this way, we have isolated the thermodynamical quantities on the right-hand side of (3.24) and the kinematical quantities on the left-hand side, which can then be integrated analytically. For some particular cases (for example when the sound speed is constant), the right-hand side too is integrable, but for a generic EOS, a numerical integration is necessary. The velocity at the tail of the rarefaction wave can then be obtained directly as

$$v_b^x = \tanh\mathscr{B}, \tag{3.25}$$

where

$$\mathscr{B} \equiv \tfrac{1}{2}\log\left(\frac{1+v_a^x}{1-v_a^x}\right) \pm \int_{p_a}^{p_*}\frac{\sqrt{h^2+\mathscr{A}^2\left(1-c_s^2\right)}}{(h^2+\mathscr{A}^2)}\frac{\mathrm{d}p}{\rho\ c_s}. \tag{3.26}$$

Here, $h = h(p,s)$, $\rho = \rho(p,s)$ and $c_s = c_s(p,s)$, and the isentropic character of rarefaction waves allows us to fix $s = s_a$. Despite its complicated appearance, the

integrand is a smooth, monotonic function of p, and a Gaussian quadrature with only 10–20 points has proved to be more accurate and efficient than a third-order Runge–Kutta integrator requiring hundreds of function evaluations to solve (3.20).

4. Limiting relative velocities

As mentioned in the previous sections, the basic operation in our approach consists of calculating the relative normal velocity across the two initial states and comparing it with the limiting relative velocities for each of the three possible wave patterns. In practice, this amounts to calculating (3.6), making use of expressions (3.4) and (3.5). In the following, we will briefly discuss the guidelines for the evaluation of the limiting relative velocities. In doing so, we will adopt the convention of paper I and assume that $p_1 > p_2$, with the x-axis normal to the discontinuity surface being positively oriented from 1 to 2.

4.1. $1\ \mathscr{S}_{\leftarrow}\ 3\ \mathscr{C}\ 3'\ \mathscr{S}_{\rightarrow}\ 2$: *two shock waves*

We first consider a wave pattern in which two shock waves propagate in opposite directions. In this case, the general expression for the relative normal velocities between the two initial states $(v^x_{12})_{2S}$ can be calculated from (3.6) with the velocities behind the shock waves v^x_3 and $v^x_{3'}$ being determined through the jump condition (3.13). Because p_1 is the smallest value that the pressure at the contact discontinuity p_3 can take, the limiting value for the two shock waves branch $(\tilde{v}^x_{12})_{2S}$ can be expressed as

$$\left(\tilde{v}^x_{12}\right)_{2S} = \lim_{p_3 \to p_1} \left(v^x_{12}\right)_{2S}. \tag{4.1}$$

Evaluating the limit (4.1) involves calculating the limits of $v^x_{1,\mathscr{C}}$ and $v^x_{2,\mathscr{C}}$ for p_3 tending to p_1. Both these limits are straightforward to calculate and are

$$\lim_{p_3 \to p_1} v^x_{1,\mathscr{C}} = 0, \tag{4.2}$$

$$\lim_{p_3 \to p_1} v^x_{2,\mathscr{C}} = \frac{v^x_2 - \bar{v}^x_{3'}}{1 - v^x_2 \bar{v}^x_{3'}}, \tag{4.3}$$

where $\bar{v}^x_{3'}$ is simply the value of v^x_3 for $p_3 = p_1$, i.e.

$$\bar{v}^x_{3'} \equiv \lim_{p_3 \to p_1} v^x_{3'}. \tag{4.4}$$

Using now the limits (4.2)–(4.3) and some lengthy but straightforward algebra, the explicit analytic expression for the limiting value of the two shock waves branch can be calculated as

$$\left(\tilde{v}^x_{12}\right)_{2S} = -\lim_{p_3 \to p_1} v^x_{2,\mathscr{C}} = \frac{(p_1 - p_2)\left(1 - v^x_2 \bar{V}_s\right)}{(\bar{V}_s - v^x_2)\left\{h_2 \rho_2 (W_2)^2 \left[1 - \left(v^x_2\right)^2\right] + p_1 - p_2\right\}}. \tag{4.5}$$

Here, $\bar{V}_s$ is the velocity of the shock wave propagating towards the right in the limit of $p_3 \to p_1$ and an explicit expression for it can be found in Appendix B in the case of an ideal fluid. Equation (4.5) will be discussed further in § 5, but it is sufficient to point out here that the threshold value $(\tilde{v}^x_{12})_{2S}$ does not depend on the initial velocity in the state 1, v_1.

4.2. $1\ \mathscr{R}_{\leftarrow}\ 3\ \mathscr{C}\ 3'\ \mathscr{S}_{\rightarrow}\ 2$: *one shock and one rarefaction wave*

We next consider the wave pattern consisting of a rarefaction wave propagating towards the left and of a shock wave propagating towards the right. Also in this

case, $(v_{12}^x)_{SR}$ can be calculated from (3.6) with $v_{3'}^x$ being determined through the jump condition (3.13) and v_3^x from the numerical integration of (3.20) in the range $[p_1, p_3]$. Because p_2 is now the lowest pressure in the unknown region behind the two nonlinear waves, the limiting value for the one shock and one rarefaction waves branch $(\tilde{v}_{12}^x)_{SR}$ can be expressed as

$$\left(\tilde{v}_{12}^x\right)_{SR} = \lim_{p_3 \to p_2} \left(v_{12}^x\right)_{SR}. \tag{4.6}$$

In the limit $p_3 \to p_2$, the right-propagating shock is suppressed, $v_{3'}^x \to v_2^x$ so that

$$\lim_{p_3 \to p_2} v_{2,\mathscr{C}}^x = 0, \tag{4.7}$$

and

$$\left(\tilde{v}_{12}^x\right)_{SR} = \lim_{p_3 \to p_2} v_{1,\mathscr{C}}^x. \tag{4.8}$$

Defining now

$$\mathscr{B}_1 \equiv \tfrac{1}{2} \log\left(\frac{1 + v_1^x}{1 - v_1^x}\right), \tag{4.9}$$

and using (3.25), it is readily obtained that

$$\left(\tilde{v}_{12}^x\right)_{SR} = \lim_{p_3 \to p_2} \tanh(\mathscr{B}_1 - \mathscr{B}) = \tanh\left(\int_{p_1}^{p_2} \frac{\sqrt{h^2 + \mathscr{A}_1^2\left(1 - c_s^2\right)}}{\left(h^2 + \mathscr{A}_1^2\right)\rho\ c_s}\, \mathrm{d}p\right), \tag{4.10}$$

where the above integral can be evaluated numerically. A closer look at the integral shows that only quantities in the left state are involved (through the constant $\mathscr{A}_1 \equiv h_1 W_1 v_1^t$) and that $(\tilde{v}_{12}^x)_{SR}$ does not depend on the initial velocity in the state 2, v_2. This property has an important consequence that will be discussed in § 5.

4.3. 1 $\mathscr{R}_{\leftarrow}$ 3 $\mathscr{C}$ 3′ $\mathscr{R}_{\rightarrow}$ 2: *two rarefaction waves*

When the wave pattern consists of two rarefaction waves propagating in opposite directions, $(v_{12}^x)_{2R}$ can be calculated from (3.6) with the velocities behind the waves being calculated using (3.25) and (3.26). Since the lowest value of the pressure behind the tails of the rarefaction waves is zero, the limiting value for the two rarefaction waves branch $(\tilde{v}_{12}^x)_{2R}$ is given by

$$\left(\tilde{v}_{12}^x\right)_{2R} = \lim_{p_3 \to 0} \left(v_{12}^x\right)_{2R}. \tag{4.11}$$

Proceeding as in § 4.2, we can now express $(\tilde{v}_{12}^x)_{2R}$ as

$$\left(\tilde{v}_{12}^x\right)_{2R} = \frac{\bar{v}_{1,\mathscr{C}}^x - \bar{v}_{2,\mathscr{C}}^x}{1 - \left(\bar{v}_{1,\mathscr{C}}^x\right)\left(\bar{v}_{2,\mathscr{C}}^x\right)}, \tag{4.12}$$

where

$$\bar{v}_{1,\mathscr{C}}^x = \tanh\left(\int_{p_1}^{0} \frac{\sqrt{h^2 + \mathscr{A}_1^2\left(1 - c_s^2\right)}}{\left(h^2 + \mathscr{A}_1^2\right)\rho\ c_s}\, \mathrm{d}p\right), \tag{4.13}$$

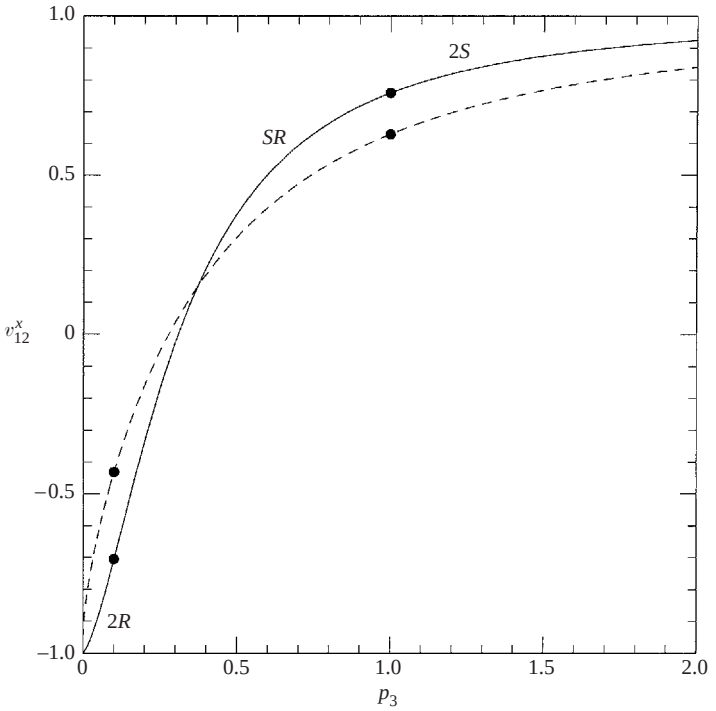

FIGURE 1. Relative normal velocity between the two initial states as a function of the pressure at the contact discontinuity. Each curve is the continuous joining (marked by solid dots) of three different curves corresponding to two shock waves ($2S$), one shock and one rarefaction wave (SR), and two rarefaction waves ($2R$). —, zero tangential velocities; - - -, $v_1^t = 0.7 = v_2^t$. The initial state vectors are those of Sod's problem. $p_1 = 1.0$, $\rho_1 = 1.0$, $p_2 = 0.1$, $\rho_2 = 0.125$.

$$\bar{v}_{2,\mathscr{C}}^x = \tanh\left(\int_0^{p_2} \frac{\sqrt{h^2 + \mathscr{A}_2^2\left(1 - c_s^2\right)}}{\left(h^2 + \mathscr{A}_2^2\right)\rho\ c_s}\,\mathrm{d}p\right), \tag{4.14}$$

and where $\mathscr{A}_2 \equiv h_2 W_2 v_2^t$. While the determination of $(\tilde{v}_{12}^x)_{2R}$ requires the numerical calculation of the integrals (4.13) and (4.14), it has very little practical importance as it marks the transition to a wave pattern with two rarefaction waves separated by a vacuum; this is a very rare physical configuration which cannot be handled by a generic numerical code.

Note that in computing (4.12), both the left and right state quantities are involved and, as a result, $(\tilde{v}_{12}^x)_{2R}$ will depend on both v_1 and v_2. This property will be important in the discussion in § 5.

Figure 1 shows the functional behaviour of $v_{12}^x = v_{12}^x(p_3)$ and how this behaviour is changed by the presence of non-zero tangential velocities. The initial conditions are those of a modified Sod's problem (Sod 1978) in which $p_1 = 1.0$, $\rho_1 = 1.0$, $v_1^x = 0.0$, $p_2 = 0.1$, $\rho_2 = 0.125$, $v_2^x = 0.0$, and $\gamma = \frac{5}{3}$. Each of the two curves shown is composed of three different curves (joined at the solid dots) corresponding to wave patterns consisting of two shock waves ($2S$), one shock and one rarefaction wave (SR), and two rarefaction waves ($2R$). While the solid curve refers to initial conditions with zero tangential velocities, the dashed curve is produced when non-zero tangential velocities, $v_1^t = 0.7 = v_2^t$, are considered. Note that also in this latter case, the

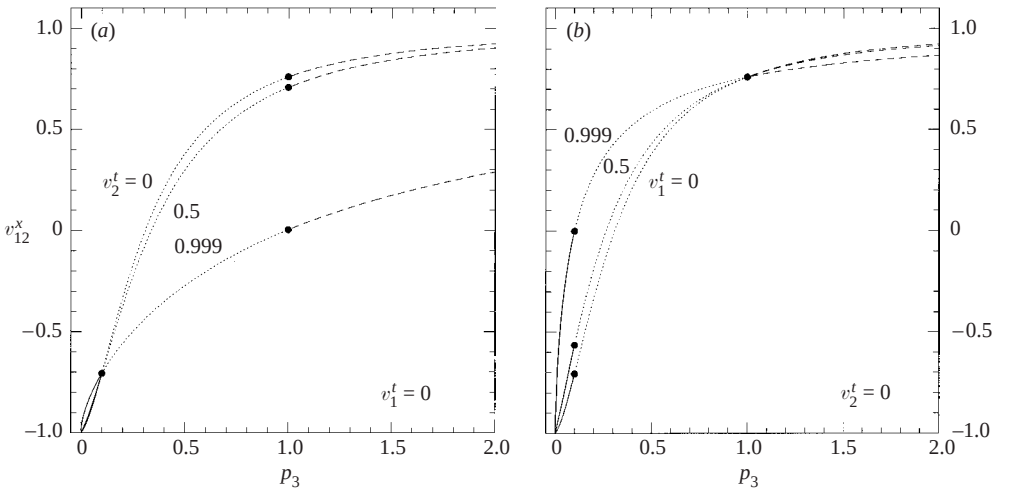

FIGURE 2. The same as in figure 1, but here the different line types mark the different branches corresponding to ---, two shock waves ···, one shock and one rarefaction wave; —, two rarefaction waves. The functional behaviour is modified when only one of the initial tangential velocities is varied (*a*) v_2^t, (*b*) v_1^t, while all the other components of the initial state vectors are unchanged.

three branches are monotonically increasing with p_3 (a fundamental property whose mathematical proof can be found in Appendix A) but are all altered by the presence of non-zero tangential velocities. The consequences of this will be discussed in the next section.

5. Relativistic effects

The changes in the functional behaviour of $v_{12}^x = v_{12}^x(p_3)$ introduced by non-zero initial tangential velocities suggest that new qualitative differences could be found in a Riemann problem with multi-dimensional relativistic flows. This was first discussed in Rezzolla & Zanotti (2002) where the basic features of new relativistic effects were briefly pointed out. This section is dedicated to a more detailed discussion of how the changes in the functional behaviour of $v_{12}^x = v_{12}^x(p_3)$ are responsible for relativistic effects in the dynamics of nonlinear waves. Before entering into the heart of the discussion, however, it is useful to remind ourselves that in Newtonian hydrodynamics a Riemann problem with multi-dimensional flows does not depend on the values of the tangential velocities at the two initial states. Rather, different wave patterns can be produced only after a suitable change in either the normal velocity, the rest-mass density or the pressure. This is essentially because tangential velocities are not changed across Newtonian nonlinear waves. In relativistic hydrodynamics, on the other hand, this is not the case and is the origin of the effects discussed below.

Let us restrict our attention to a situation in which the tangential velocity of only one of the two initial states is varied. This is simpler than the general case as it represents a one-dimensional cross-section of the three-dimensional parameter space, but it maintains all of the relevant properties. Figure 2 shows the relative normal velocity for the same initial conditions of figure 1 where either v_1^t or v_2^t is varied while all the other quantities of the initial state vectors are unchanged. Different line types mark the different branches (joined at the filled dots) describing the relative velocity

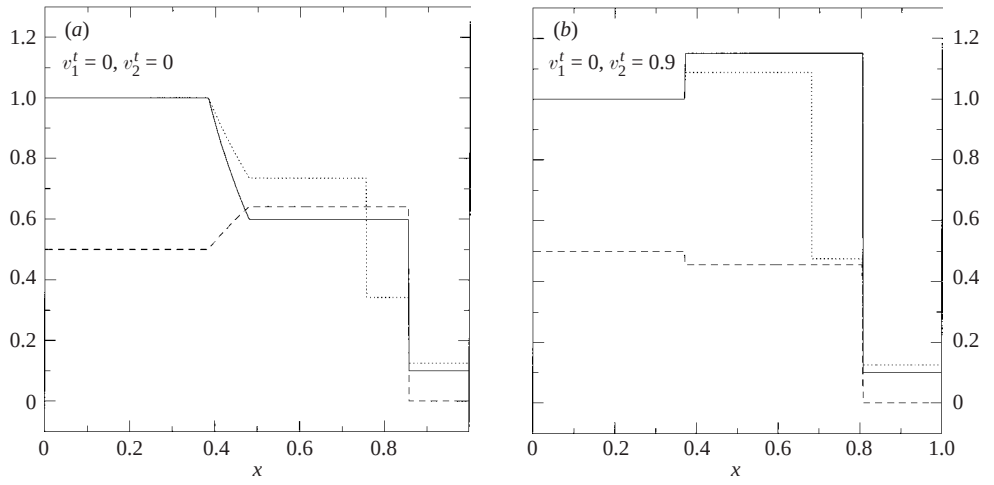

FIGURE 3. Transition from an SR wave pattern to a $2S$ one. (a) and (b) show the exact solution of the Riemann problem corresponding to models (a) and (e) in table 1, respectively. The initial-state vectors are identical except for the values of v_2^t. —, p; $\cdots$, ρ; ---, v^x.

corresponding to two shock waves ($2S$, dashed line), one shock and one rarefaction wave (SR, dotted line), and two rarefaction waves ($2R$, continuous line), respectively. Figure 2 indicates that when tangential velocities are present, the relative normal velocity is a function of p_3 but also of v_1^t and v_2^t.

Consider, for instance, the case in which the normal velocities are chosen to be $v_1^x = 0.5$, $v_2^x = 0$, and that there are no tangential velocities. In this case, $(v_{12}^x)_0 = 0.5$ and figure 2(a) shows that the solution to the Riemann problem falls in the SR branch, hence producing a wave pattern consisting of a shock and a rarefaction wave moving in opposite directions. This is shown in more detail in figure 3(a) where the different types of line show the solution of the Riemann problem at a time $t > 0$ for the pressure (continuous line), the rest-mass density (dotted line) and the velocity (dashed line).

However, if we now maintain the same initial conditions, but allow for non-zero tangential velocities in state 2, figure 2(a) also shows that the solution to the Riemann problem can fall in the $2S$ branch, hence producing a wave pattern consisting of two shock waves moving in opposite directions. This is shown in figure 3(b) which illustrates the solution of the same Riemann problem, but with initial tangential velocities $v_1^t = 0$ and $v_2^t = 0.9$. Note that except for the tangential velocities, the solutions in figure 3 have the same initial-state vectors, but different intermediate ones (i.e. p_3, ρ_3, $\rho_{3'}$ and v_3^x).

The Riemann problem shown in figure 3 is only one possible example, but shows that a change in the tangential velocities can produce a smooth transition from one wave pattern to another while maintaining the initial states unmodified. Furthermore, because the coupling among the different states is produced by the Lorentz factors, this is not sensitive on the sign chosen for the tangential velocity. The transition from one wave pattern to the other is illustrated better in figure 4 where we have collected in a three-dimensional plot a sequence of solutions for the pressure in which v_2^t is gradually increased from 0 to 0.9. Note that when $v_2^t = 0$, the SR wave pattern is well defined and the pressure at the contact discontinuity is intermediate between p_1 and

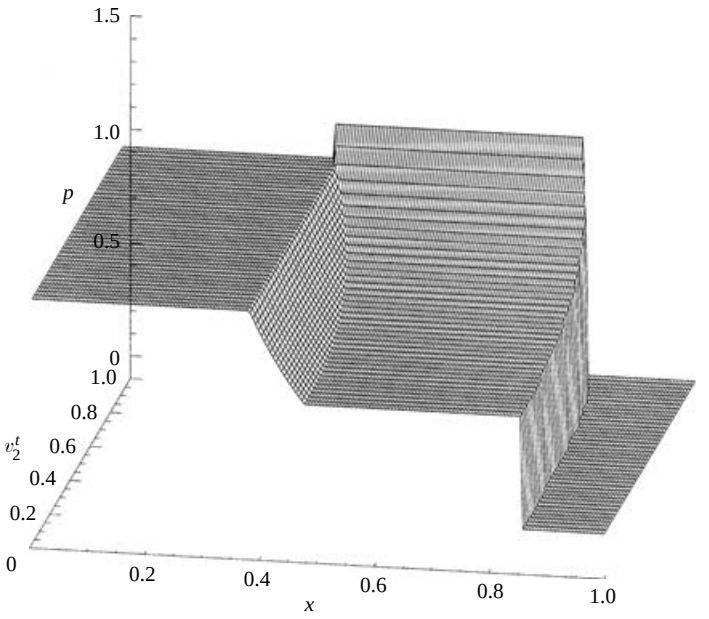

FIGURE 4. Sequence of solutions for the pressure in Sod's problem. The initial tangential velocity v_2^t is gradually increased from 0 to 0.9. The first and last solutions of this sequence are also plotted in figure 3.

p_2. Note also that as v_2^t is increased, the wave pattern gradually changes, p_3 increases until it becomes larger than p_1, signalling the transition to a $2S$ wave pattern.

The transition does not always produce a solution consisting of two shock waves. Suppose, in fact, that the normal velocities are now chosen to be $v_1^x = 0,\ v_2^x = 0.5$. We can repeat the considerations made above and start by examining the wave pattern produced when there are zero tangential velocities. In this new set-up, $(v_{12}^x)_0 = -0.5$ and figure 2(b) shows that the solution to the Riemann problem still falls in the SR branch (cf. dashed line), with the corresponding solution at a time $t > 0$ being presented in figure 5(a). (Note that the wave patterns in figures 3 and 5 both consist of a shock and a rarefaction wave, but have alternating initial normal velocities.)

When non-zero tangential velocities are now considered in state 1, figure2(b) shows that $(v_{12}^x)_0$ can fall in the $2R$ branch, hence producing a wave pattern consisting of two rarefaction waves moving in opposite directions. The solution to this Riemann problem is shown in figure 5(b) where we have chosen initial tangential velocities $v_1^t = 0.999$ and $v_2^t = 0$. In this case too, it should be noted that, except for the tangential velocities, the solutions in figure 5 have the same initial-state vectors, but different intermediate ones.

In analogy with figure 4, we have collected in figure 6 a sequence of solutions for the pressure in which v_1^t is gradually increased from 0 to 0.999. Here too, when $v_2^t = 0$, the SR wave pattern is well defined and the pressure at the contact discontinuity is intermediate between p_1 and p_2. However, as v_1^t is increased, the wave pattern gradually changes, p_3 decreases until it becomes smaller than p_2, signalling the transition to a $2R$ wave pattern. Note that while this happens, the region of the flow covered by the rarefaction wave becomes progressively smaller.

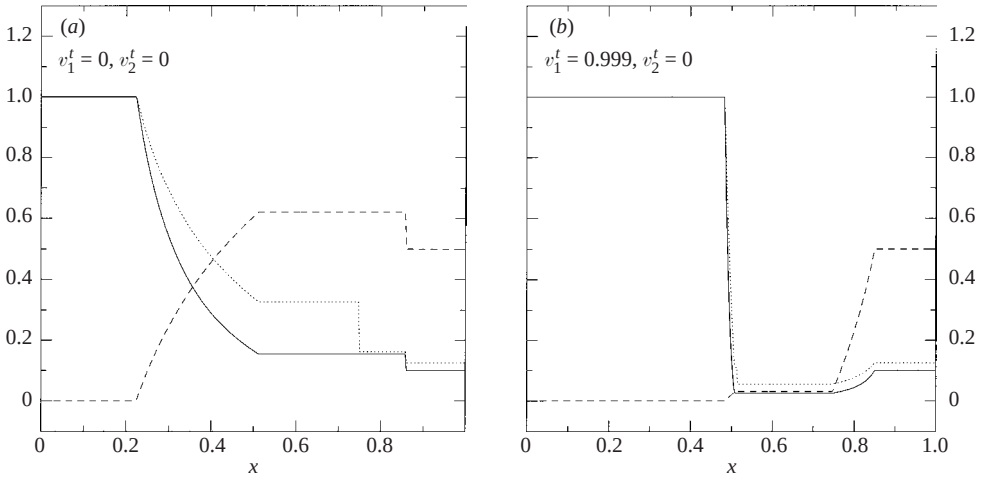

FIGURE 5. The same as in figure 3, but for models (*h*) and (*n*) in table 1. Also, in this case, the initial-state vectors are identical except for the values of v_1^t. Note that in (*b*), the left-propagating rarefaction wave covers a very small region of the flow and is closely followed by the contact discontinuity.

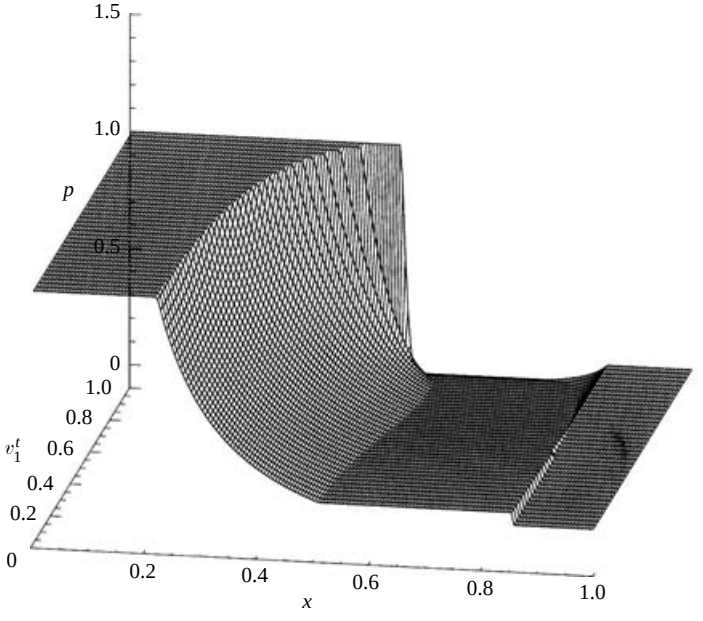

FIGURE 6. The same as in figure 4, but here the initial tangential velocity v_1^t is gradually increased from 0 to 0.999. The first and last solutions of this sequence are also plotted in figure 5.

In table 1 we have summarized a few of the solutions shown in figures 4 and 6, presenting numerical values for all of the relevant quantities in the Riemann problem when different combinations of the tangential velocities are used.

The transformation of a rarefaction wave into a shock wave and vice versa can also be appreciated by considering how the velocities at which the various nonlinear waves propagate in the unperturbed media change when the tangential velocities v_1^t and

Model	v_1^x	v_2^x	v_1^t	v_2^t	p_*	v_*^x	ρ_3	$\rho_{3'}$	Wave pattern
(*a*)	0.5	0.0	0.0	0.000	0.597	0.640	0.734	0.342	*SR*
(*b*)	0.5	0.0	0.0	0.300	0.621	0.631	0.751	0.349	*SR*
(*c*)	0.5	0.0	0.0	0.500	0.673	0.611	0.788	0.364	*SR*
(*d*)	0.5	0.0	0.0	0.700	0.787	0.570	0.866	0.394	*SR*
(*e*)	0.5	0.0	0.0	0.900	1.150	0.455	1.088	0.474	*2S*
(*f*)	0.5	0.0	0.0	0.990	2.199	0.212	1.593	0.647	*2S*
(*g*)	0.5	0.0	0.0	0.999	3.011	0.078	1.905	0.750	*2S*
(*h*)	0.0	0.5	0.000	0.0	0.154	0.620	0.326	0.162	*SR*
(*i*)	0.0	0.5	0.300	0.0	0.139	0.594	0.306	0.152	*SR*
(*j*)	0.0	0.5	0.500	0.0	0.115	0.542	0.274	0.136	*SR*
(*k*)	0.0	0.5	0.700	0.0	0.085	0.450	0.228	0.113	*2R*
(*l*)	0.0	0.5	0.900	0.0	0.051	0.280	0.168	0.084	*2R*
(*m*)	0.0	0.5	0.990	0.0	0.031	0.095	0.123	0.061	*2R*
(*n*)	0.0	0.5	0.999	0.0	0.026	0.031	0.110	0.052	*2R*

TABLE 1. Solution of the modified Sod's problem at $t = 0.4$. All models refer to an ideal EOS with $\gamma = \frac{5}{3}$ and share the same values of pressure and rest-mass density: $p_1 = 1.0$, $\rho_1 = 1.0$, $p_2 = 0.1$, $\rho_2 = 0.125$. The only differences present in the problems considered are in the normal relative velocity and in the tangential velocities. These quantities are reported in the first three columns, and the remaining ones show a few relevant quantities of the solution in the newly formed region as well as the wave pattern produced.

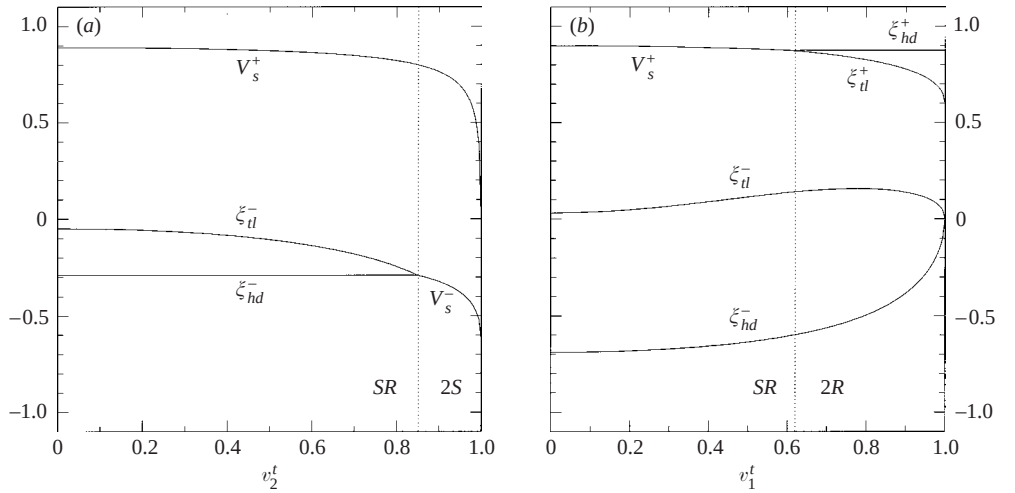

FIGURE 7. Velocities of the various nonlinear waves when the tangential velocities v_1^t and v_2^t are varied separately. The initial conditions are those of Sod's problem and the different curves refer to the head and tail of a left-propagating rarefaction wave (i.e. ξ_{tl}^-, ξ_{hd}^-), to the head and tail of a right-propagating rarefaction wave (i.e. ξ_{tl}^+, ξ_{hd}^+), and to a left or a right-propagating shock wave (i.e. V_s^-, V_s^+).

v_2^t are varied separately. This information is contained in figure 7 in which different curves show the behaviour of the head and tail of a left-propagating rarefaction wave (i.e. ξ_{tl}^-, ξ_{hd}^-), of the head and tail of a right-propagating rarefaction wave (i.e. ξ_{tl}^+, ξ_{hd}^+), and of a left- or a right-propagating shock wave (i.e. V_s^-, V_s^+). Figure 7(*a*), in particular, shows the transition from a *SR* to a 2*S* wave pattern with the dotted vertical line marking the value of v_2^t at which this occurs. Similarly, figure 7(*b*) shows

the transition from an SR to a $2R$ wave pattern and the dotted vertical line is again used to mark the limiting value of v_1^t.

The effects discussed in this section have a purely special relativistic origin. They might conflict with our physical intuition, especially when the latter is based on the knowledge of the Riemann problem in Newtonian hydrodynamics. However, the behaviour reported here is typical of those special relativistic phenomena involving Lorentz factors including also tangential velocities. A useful example in this respect is offered by the relativistic transverse-Doppler effect, in which the wavelength of a photon received from a source moving at relativistic speeds changes also if the source has a velocity component orthogonal to the direction of emission of the photon (Rindler 1982). In this case too, a Lorentz factor including the transverse velocity is responsible for the effect.

Finally, it should be pointed out that there exists a set of initial conditions for which these new relativistic effects cannot occur. These initial conditions are those in which $v_1^x = v_2^x$ as in the classic 'shock-tube' problem, where $v_1^x = 0 = v_2^x$. In this case, in fact, $(v_{12}^x)_0 = 0$ and the solution of the Riemann problem will be given by a wave pattern consisting of a shock and a rarefaction wave, independently of the values of the tangential velocities (cf. limits (A 2) and (A 4 in Appendix A).

6. Conclusions

We have shown that an efficient solution of the exact Riemann problem in multidimensional relativistic flows can be obtained after exploiting the properties of the invariant expression for the relative normal velocity between the two initial states. The new procedure proposed here is the natural extension of a similar method presented for the exact solution of the Riemann problem in one-dimensional relativistic flows (Rezzolla & Zanotti 2001). Using information contained in the initial-state vectors, this approach predicts the wave pattern that will be produced in the Riemann problem, determines the set of equations to be solved and brackets the interval in pressure where the solution should be sought. Because it is logically straightforward, this approach results in an algorithm which is very easy to implement numerically and work is now in progress to assess the computational speed-up in multidimensional codes.

An important aspect of this strategy is that it naturally points out relativistic effects that can take place whenever the initial relative velocity normal to the initial surface of discontinuity is non-zero. When this is the case, in fact, the tangential velocities can affect the solution of the Riemann problem and cause a transition from one wave pattern to another. More specifically, by varying the tangential velocities on either side of the initial discontinuity while keeping the remaining state vectors unchanged, the nonlinear waves involved in the solution Riemann problem can change from rarefaction waves to shock waves and vice versa. These effects have a purely relativistic nature, do not have a Newtonian counterpart and could be relevant in several astrophysical scenarios, such as those involving relativistic jets or γ-ray bursts, in which nonlinear hydrodynamical waves with large Lorentz factors and complex multidimensional flows are expected (Blandford 2002; Meszaros 2002).

As a final remark, it is worth pointing out that while the content of this paper is focused on special relativistic hydrodynamics and flat space–times, the local Lorentz invariance allows us to extend the results discussed here also to curved space–times and general relativistic numerical calculations (Pons *et al.* 1998; and Font 2000 for a review).

It is a pleasure to thank J. C. Miller and J. M. Ibáñez for useful discussions and comments. Financial support for this work has been provided by the Italian MIUR and by the EU Programme 'Improving the Human Research Potential and the Socio-Economic Knowledge Base' (Research Training Network Contract HPRN-CT-2000-00137). J. A. P. is supported by Marie Curie Fellowship no. HPMF-CT-2001-01217.

Appendix A. Monotonicity of the relative velocity as function of p_*

This Appendix is devoted to the proof that v_{12}^x is a monotonic function of p_*; as mentioned in the main text, this is an important property and the basis of our approach.

With our choice of considering the initial left state as the one with highest pressure, the proof of monotonicity will be obtained if we show that v_{12}^x is a monotonically *increasing* function of p_*. Indicating then with a prime the first derivative with respect to p_* and dropping the upper index x in the notation for the normal velocities, it is straightforward to derive that the first derivative of expression (3.6) is given by

$$v'_{12} = \frac{v'_{1,\mathscr{C}}\left(1 - v^2_{2,\mathscr{C}}\right) - v'_{2,\mathscr{C}}\left(1 - v^2_{1,\mathscr{C}}\right)}{\left(1 - v_{1,\mathscr{C}}\, v_{2,\mathscr{C}}\right)^2}. \tag{A 1}$$

Equation (A 1) suggests that the proof that v_{12}^x is monotonically increasing will follow if it can be shown that $v'_{1,\mathscr{C}}$ and $-v'_{2,\mathscr{C}}$ are both positive. On the other hand, using (3.4) and (3.5), the proof of the monotonicity will follow from showing that $(v_3^x)' < 0$ and $(v_{3'}^x)' > 0$. While these inequalities must hold irrespective of the nonlinear wave considered, the proofs will be different for the different waves considered.

When a rarefaction wave is present, the proof is indeed straightforward. According to (3.20) and (3.23), in fact, $(v^x)'$ across the rarefaction wave is negative when the rarefaction wave propagates towards the left (implying that $(v_3^x)'$ is negative) and it is positive when the rarefaction wave propagates towards the right (implying that $(v_{3'}^x)'$ is positive).

If a shock wave is present, on the other hand, a proof for the most general case and in terms of simple algebraic relations cannot be given. On the other hand, a rather simple analytic proof can be found in the simpler case in which $v_1^x = v_2^x = 0$; while this is certainly not the most general case, numerical calculations have shown that the result holds in general. Consider therefore a shock wave propagating towards the left (a similar analysis can be repeated for the right-propagating shock wave); after lengthy but straightforward calculations, it is possible to show that

$$(v_3^x)' = \frac{H_1\left(V_s - v_1^x\right)\left(1 - V_s v_1^x\right) - H_1 \Delta p\left(1 - \left(v_1^x\right)^2\right) V_s' - V_s'(\Delta p)^2}{\left[H_1\left(V_s - v_1^x\right) + \Delta p V_s\right]^2}, \tag{A 2}$$

where we have set $H_1 \equiv h_1 \rho_1 W_1^2$ and $\Delta p \equiv p - p_1 > 0$, and where p is the pressure behind the shock. If we now impose that $v_1^x = 0$, we can write the derivative of (3.12) as

$$\frac{V_s'}{V_s} = \frac{J'}{J}\frac{\rho_1^2 W_1^2}{J^2 + \rho_1^2 W_1^2}. \tag{A 3}$$

Substituting (A 3) into (A 2), we can conclude that $(v_3^x)'$ is negative if and only if

$$J\left(\rho_1^2 W_1^2 + J^2\right) h_1 - \rho_1 \Delta p J'\left(\rho_1 h_1 W_1^2 + \Delta p\right) < 0. \tag{A 4}$$

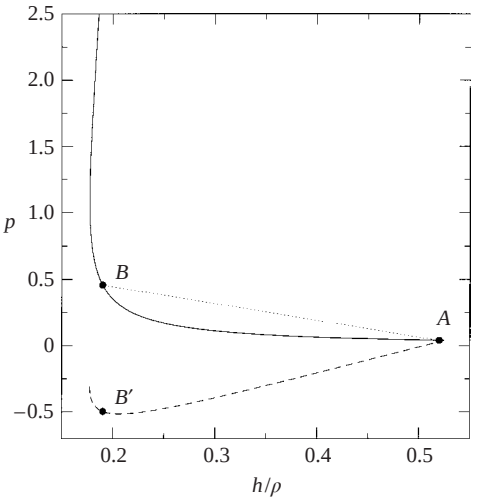

FIGURE 8. —, the Taub adiabat. A, B, the states ahead of and behind a left-propagating shock wave. See the main text for a discussion.

Using (3.17) to calculate J', we find that (A 4) can be written as

$$-\frac{\rho_1(H_1-\Delta p)}{J^2}-2h_1<\frac{1}{\gamma(\gamma-1)}\frac{\rho_1(H_1+\Delta p)}{\rho^2}\left[\frac{1}{\epsilon}-\gamma(\gamma-2)\right], \tag{A 5}$$

where ρ and ϵ are the rest-mass density and the specific internal energy behind the shock front. Because the right-hand side of (A 5) is always positive for any $\gamma \leqslant 2$, the condition for monotonicity, (A 5), will be satisfied if its left-hand side is negative, i.e. if

$$-J^2<-\rho_1\frac{\Delta p-H_1}{2h_1}\equiv-\alpha. \tag{A 6}$$

At this point, the proof can be continued graphically and by making use of the Taub adiabat. In the plane $(h/\rho, p)$, in fact, the Taub adiabat (3.18) selects the points solutions of the hydrodynamical equations across a shock wave, therefore connecting the state ahead of the shock front with the one behind it. In figure 8, this curve is shown as a solid line and we have indicated with the points A and B the states ahead (region 1) and behind (region 3) the shock front. Once an initial state A has been chosen, the mass flux will determine the point B of the Taub adiabat solution of the Rankine–Hugoniot relations. Because of this, the slope of the chord connecting the points A and B (shown as a dotted line in figure 8) is equal to $-J^2$. The dashed line in figure 8 shows the equivalent of the Taub adiabat passing through the state A, but having mass flux equal to $\alpha^{1/2}$, i.e.

$$p=-\alpha\left(\frac{h}{\rho}-\frac{h_1}{\rho_1}\right)+p_1. \tag{A 7}$$

The point B' on such a curve represents the state behind the shock wave and, as is clearly shown in figure 8, the slope of the chord AB' is always larger than the corresponding slope for the chord AB, thus stating that the condition (A 5) is indeed verified and that $(v_3^x)'$ is therefore positive.

Appendix B. Dependence of the limiting values on the tangential velocities

As mentioned in § 5, the appearance of the new relativistic effects is related to the behaviour of the function $v_{12}^x = v_{12}^x(p_3)$ for different values of the initial tangential velocities and in particular to how the three branches composing the curve change under variation of $v_{1,2}^t$. As a result, the occurrence of these effects can be recast into the study of the dependence of $(\tilde{v}_{12}^x)_{2S}$, $(\tilde{v}_{12}^x)_{SR}$ and $(\tilde{v}_{12}^x)_{2R}$ on the tangential velocities. Using expressions (4.5), (4.10) and (4.12), this dependence can be summarized as follows

$$\left(\tilde{v}_{12}^x\right)_{2S} = \left(\tilde{v}_{12}^x\right)_{2S}\left(v_2^t\right), \qquad \left(\tilde{v}_{12}^x\right)_{SR} = \left(\tilde{v}_{12}^x\right)_{SR}\left(v_1^t\right), \quad \left(\tilde{v}_{12}^x\right)_{2R} = \left(\tilde{v}_{12}^x\right)_{2R}\left(v_1^t, v_2^t\right), \tag{B 1}$$

and can be best studied by considering the limits of $(\tilde{v}_{12}^x)_{2S}$, $(\tilde{v}_{12}^x)_{SR}$ and $(\tilde{v}_{12}^x)_{2R}$ when $W_{1,2} \to \infty$. In the case of a $2S$ wave pattern, (4.5) simply indicates that

$$\lim_{W_2 \to \infty} \left(\tilde{v}_{12}^x\right)_{2S} = 0. \tag{B 2}$$

This result is also shown in figure 2(*a*), where the right solid dot converges to zero as $W_2 \to \infty$, while the left one does not vary. The limit (B 2) can also be used to deduce that for any $(v_{12}^x)_0 > 0$, there exists a value $\bar{W}_2$ of W_2 such that

$$\left(v_{12}^x\right)_0 > \left(\tilde{v}_{12}^x\right)_{2S} \quad \text{for} \quad W_2 > \bar{W}_2. \tag{B 3}$$

A direct consequence of (B 3) is that given a Riemann problem having initial-state vectors with positive relative normal velocity and producing an SR wave pattern, it is always possible to transform it into a $2S$ wave pattern by increasing the value of the initial tangential velocity in the state of initial lower pressure.

In the case of an SR wave pattern, we refer to (4.10) to see that in the limit of $W_1 \to \infty$ the integrand vanishes ($\mathscr{A}_1 \to \infty$) and therefore:

$$\lim_{W_1 \to \infty} \left(\tilde{v}_{12}^x\right)_{SR} = 0. \tag{B 4}$$

As for the previous one, the limit (B 4) can be deduced from figure 2(*b*), where the left solid dot converges to zero as $W_1 \to \infty$, while the right one does not vary. Also in this case, the limit (B 4) can be used to conclude that for any $(v_{12}^x)_0 < 0$, there exists a value $\bar{W}_1$ of W_1 such that

$$\left(v_{12}^x\right)_0 < \left(\tilde{v}_{12}^x\right)_{SR} \quad \text{for} \quad W_1 > \bar{W}_1, \tag{B 5}$$

and therefore causing an initial SR wave-pattern solution to become a $2R$ one as a consequence of an increased tangential velocity in the state of initial higher pressure.

Overall, (B 2) and (B 4) indicate that for tangential velocities assuming increasingly larger values, the SR branch of the v_{12}^x curve spans a progressively smaller interval of relative normal velocities. When the tangential velocities reach their asymptotic values, the SR branch reduces to a point. In practice, therefore, the main effect introduced by relativistic tangential velocities in a Riemann problem is that of disfavouring the occurrence of a wave pattern consisting of a shock and a rarefaction wave.

For completeness, we also report the limit of the relative normal velocity marking the branch of two rarefaction waves separated by a vacuum. In this case, the limit is taken for both W_1 and W_2 tending to infinity, and using (4.13)–(4.14) yields

$$\lim_{W_{1,2} \to \infty} \left(\tilde{v}_{12}^x\right)_{2R} = 0. \tag{B 6}$$

Appendix C. An explicit expression for $\bar{V}_s$

In this Appendix, we provide an explicit expression of the velocity of the shock wave propagating towards the right in the limit of $p_3 \to p_1$ and when the fluid is ideal. This quantity, which is necessary to calculate the limiting relative velocity $(\widetilde{v}^x_{12})_{2S}$ in (4.5), can be computed easily as cf. (3.12)

$$\bar{V}_s = \frac{\rho_2^2 W_2^2 v_2^x + |J_{23'}| \sqrt{J_{23'}^2 + \rho_2^2 W_2^2 \left[1 - \left(v_2^x\right)^2\right]}}{\rho_2^2 W_2^2 + J_{23'}^2}, \tag{C 1}$$

where the mass flux $J_{23'}$ is given by (cf. (3.17))

$$J_{23'}^2 = -\left(\frac{\gamma}{\gamma - 1}\right) \frac{p_1 - p_2}{h_{3'}(h_{3'} - 1)/p_1 - h_2(h_2 - 1)/p_2}, \tag{C 2}$$

and where, finally, $h_{3'}$ is the positive root of the Taub adiabat (3.18) in the limit of $p_3 \to p_1$, i.e.

$$h_{3'} = \frac{(\sqrt{\mathscr{D}} - 1)(\gamma - 1)(p_1 - p_2)}{2[(\gamma - 1)p_2 + p_1]}, \tag{C 3}$$

where

$$\mathscr{D} = 1 - 4\gamma p_1 \frac{(\gamma - 1)p_2 + p_1}{(\gamma - 1)^2 (p_1 - p_2)^2} \left[\frac{h_2(p_2 - p_1)}{\rho_2} - h_2^2\right]. \tag{C 4}$$

REFERENCES

Anile, A. M. 1989 *Relativistic Fluids and Magneto-fluids: with Applications in Astrophysics and Plasma Physics*. Cambridge University Press.

Blandford, R. D. 2002 Black holes and relativistic jets. *Prog. Theor. Phys. Supp.* **143**, 182.

Chandrasekhar, S. 1961 *Hydrodynamic and Hydromagnetic Stability*. Dover.

Font, J. A. 2000 Numerical hydrodynamics in general relativity. *Living Rev. Relativity* **3**, 2.

Godunov, S. K. 1959 A finite difference method for the numerical computation and discontinuous solutions of the equations of fluid dynamics. *Mat. Sb.* **47**, 271.

Ibañez, J. M. & Martí, J. M. 1999 Riemann solvers in relativistic astrophysics. *J. Comput. Appl. Maths* **109** 173.

Landau, L. D. & Lifshitz, E. M. 1987 *Fluid Mechanics*, 2nd edn., §100. Pergamon.

Leveque, R. J. 1992 *Numerical Methods for Conservation Laws*. Birkhäuser.

Leveque, R. J. 2002 *Finite Volume Methods for Hyperbolic Problems*. Cambridge University Press.

Koenigl, A. 1980 Relativistic gasdynamics in two dimensions. *Phys. Fluids* **23**, 1083.

Martí, J. M., Ibañez, J. M. & Miralles, J. A. 1991 Numerical relativistic hydrodynamics: local characteristic approach. *Phys. Rev.* D **43**, 3794.

Martí, J. M. & Müller, E. 1994 The analytical solution of the Riemann problem in relativistic hydrodynamics. *J. Fluid Mech.* **258**, 317.

Martí, J. M. & Müller, E. 1999 Numerical hydrodynamics in special relativity. *Living Rev. Relativity* **2**, 3.

Meszaros, P. 2002 Theories of gamma-ray bursts. *Annu. Rev. Astron. Astrophys.* **40**, in press.

Pons, J. A., Font, J. A., Martí, J. M., Ibañez, J. M. & Miralles, J. A. 1998 General relativistic hydrodynamics with special relativistic Riemann solvers. *Astron. Astrophys.* **339**, 638.

Pons, J. A., Martí, J. M., & Müller, E. 2000 The exact solution of the Riemann problem with nonzero tangential velocities in relativistic hydrodynamics. *J. Fluid Mech.* **422**, 125.

Press, W. H., Teukolsky, S. A. Vetterling, W. T. & Flannery, B. P. 1992 *Numerical Recipes in Fortran 77*, 2nd edn. Cambridge University Press.

Rezzolla, L. & Zanotti, O. 2001 An improved exact Riemann solver for relativistic hydrodynamics. *J. Fluid Mech.* **449**, 395.

Rezzolla, L. & Zanotti, O. 2002 New relativistic effects in the dynamics of nonlinear hydrodynamical waves. *Phys. Rev. Lett.* **89**, 114 501.

Rindler, W. 1982 *Introduction to Special Relativity*. Oxford University Press.

Sod, G. A. 1978 A survey of several finite difference methods for systems of nonlinear hyperbolic conservation laws. *J. Comput. Phys.* **27**, 1.

Smoller, J. & Temple, B. 1993 Global solutions of the relativistic Euler equations. *Commun. Math. Phys.* **156**, 67.

Taub, A. H. 1948 Relativistic Rankine–Hugoniot relations, *Phys. Rev.* **74**, 328.

Toro, E. F. 1997 *Riemann Solvers and Numerical Methods for Fluid Dynamics*. Springer.